Volume 3 | Number 30 | 14 August 2015 | Pages 15341–15770

Journal of Materials Chemistry A

Materials for energy and sustainability

www.rsc.org/MaterialsA

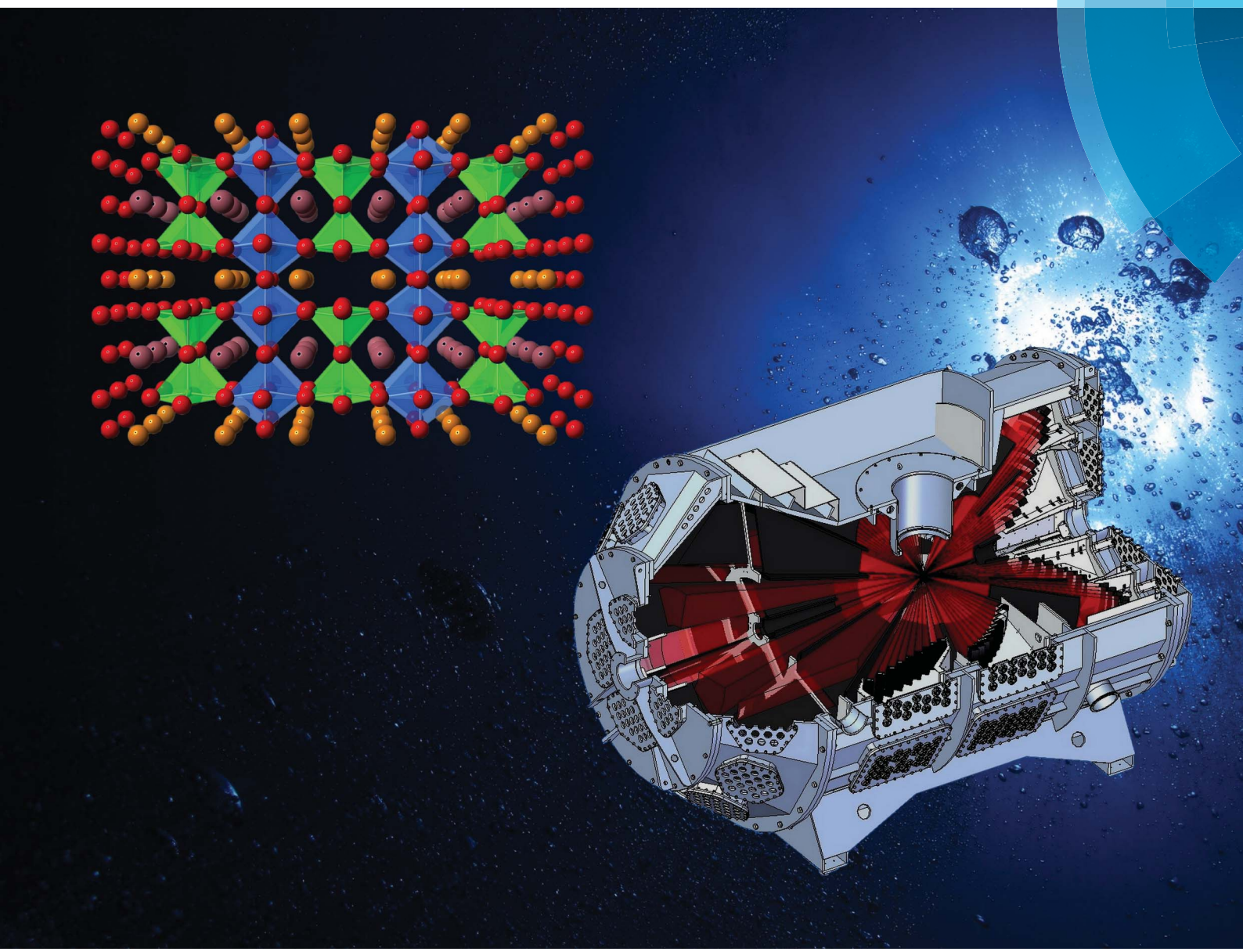

ISSN 2050-7488

ROYAL SOCIETY OF CHEMISTRY

PAPER

Mona Bahout, Stephen J. Skinner *et al.*

Stability of $NdBaCo_{2-x}Mn_xO_{5+\delta}$ (x = 0, 0.5) layered perovskites under humid conditions investigated by high-temperature *in situ* neutron powder diffraction

Journal of Materials Chemistry A

PAPER

View Article Online
View Journal | View Issue

Cite this: J. Mater. Chem. A, 2015, 3, 15420

Stability of $NdBaCo_{2-x}Mn_xO_{5+\delta}$ ($x = 0$, 0.5) layered perovskites under humid conditions investigated by high-temperature *in situ* neutron powder diffraction†

Mona Bahout,*[a] Stevin S. Pramana,[b] James M. Hanlon,[a] Vincent Dorcet,[a] Ronald I. Smith,[c] Serge Paofai[a] and Stephen J. Skinner*[b]

The double perovskites $NdBaCo_{2-x}Mn_xO_{5+\delta}$ ($x = 0$ and 0.5) were investigated using *in situ* high temperature neutron powder diffraction in dry argon and wet atmospheres (40% D_2O/argon and 40% D_2O/air) in order to assess their stability as cathodes in proton conducting fuel cells. The $x = 0$ oxide loses oxygen on heating in dry argon at $T > 400$ °C and exhibits an oxygen vacancy order–disorder transition as evidenced by the orthorhombic *Pmmm* to tetragonal *P*4/*mmm* transition. Refinement of site occupancy factors suggests that the oxygen vacancies mainly form in the Nd layers and to a lesser extent at the equatorial positions of the transition metal polyhedra; at 800 °C, $\delta \sim 0$. When the gas was changed to wet argon at 800 °C and the sample cooled to 260 °C, no structural modification or change in the oxygen content was detected and no impurity phases formed, highlighting the excellent stability of the sample in wet atmospheres. On switching the gas to wet air at 260 °C, thermal analysis and neutron powder diffraction data together reveal that the sample intercalates mainly oxygen rather than proton defects within a two-phase process involving two orthorhombic phases, reflecting the symmetry of the reduced and oxidised materials. On heating, the sample transforms at $T \geq 600$ °C to a single tetragonal phase whose symmetry is retained up to 800 °C and on subsequent cooling. The $x = 0.5$ material prepared in argon adopted a tetragonal *P*4/*mmm* structure at RT with $\delta \sim 0$. Its symmetry remains tetragonal on heating/cooling in wet argon. On changing the gas to wet air at 260 °C, it takes up oxygen *via* a two-phase process involving two tetragonal phases. Since fast oxidation is the main process that fills the oxygen vacancies of these double perovskites in wet air, a large oxygen deficiency seems to be not the only requirement for effective proton incorporation in this family of materials with basic characteristics.

Received 16th April 2015
Accepted 19th May 2015

DOI: 10.1039/c5ta02776d

www.rsc.org/MaterialsA

1. Introduction

Conventional solid oxide fuel cells (SOFCs) based on the oxide ion conducting electrolyte, 8 mol% yttria-stabilized zirconia (8YSZ), need high operating temperatures, between 800 and 1000 °C, to achieve sufficient ionic conductivity in the electrolyte.[1] Such high temperatures impose great challenges on the long-term stability and durability of SOFC materials[2] and require the use of expensive ceramic interconnects and heat exchangers. For this reason, significant research efforts are currently devoted to reducing the operation of SOFCs to the intermediate temperature (IT) range of ~400–700 °C, while retaining the benefits of elevated temperatures.[2,3] In this view, a proton conducting SOFC (H^+-SOFC) based on a proton conducting ceramic electrolyte that can operate between 300 and 600 °C has emerged as a promising candidate.[4–8] Proton conduction requires the existence of proton defects in the oxide whose incorporation into the bulk requires the presence of oxygen vacancies.[8,9] Indeed, the main reaction leading to the formation of proton defects is the dissociative adsorption of water onto a hydroxide ion and a proton; the hydroxide ion fills an oxide ion vacancy, and the proton forms a covalent bond with lattice oxygen ($H_2O_{(gas)} + V_O^{\cdot\cdot} + O_O^{\times} \leftrightarrow 2OH_O^{\cdot}$ in the Kröger–Vink notation). Proton conduction consists of the hopping of protons between neighboring oxygen positions, termed as the Grotthuss (or free-proton) mechanism.

Besides the search for suitable electrolytes combining high proton conductivity at moderate temperature with thermodynamic stability, the development of cathode materials for

[a]Institut des Sciences Chimiques de Rennes, Equipe « Chimie du Solide et Matériaux », UMR CNRS 6226, Université de Rennes 1, 263 Avenue du Général Leclerc, 35042 Rennes, France. E-mail: mona.bahout@univ-rennes1.fr

[b]Department of Materials, Imperial College London, Exhibition Road, London SW7 2AZ, UK

[c]The ISIS Facility, STFC Rutherford Appleton Laboratory, Chilton, Didcot, OX11 0QX, UK

† Electronic supplementary information (ESI) available. See DOI: 10.1039/c5ta02776d

H^+-SOFC with fast transfer kinetics in the IT range is another challenging issue.[10] The cathode plays a critical role in proton conducting fuel cells because water is produced at the cathode. Most work on H^+-SOFC has been carried out using Pt electrodes surrounded by doped cerate ($ACeO_3$) or zirconate ($AZrO_3$) proton conducting electrolytes. Despite their good catalytic activity, Pt electrodes exhibit a large overpotential and are too expensive for large-scale applications.[11] Recently, double-layered perovskite oxides, $LnBaCo_2O_{5+\delta}$ (Ln = lanthanide), have been investigated as cathodes in H^+-SOFCs.[10,12,13] These oxides were extensively studied as cathode materials for O^{2-}-SOFCs due to their excellent electrochemical properties correlated with their mixed conductivity (O^{2-}/e^-).[15,16] Their structure consists of A-site ordering into alternate layers of Ln and Ba ions with oxygen vacancies primarily located in the LnO_δ layers. A variety of unit cells were reported for $LnBaCo_2O_{5+\delta}$ compounds at various temperatures and δ ranges; the most common are $P4/mmm$ ($a_p \times a_p \times 2a_p$) and $Pmmm$ ($a_p \times 2a_p \times 2a_p$), where a_p is the lattice parameter of a simple cubic perovskite. The behaviour of $LnBaCo_2O_{5+\delta}$ compounds in wet air was previously investigated by thermogravimetric analysis (TGA). Chemical compatibility tests with the $BaZr_{0.9}Y_{0.1}O_{3-\delta}$ proton conducting electrolyte revealed no impurity phases.[12] The oxygen reduction reaction was investigated by electrochemical impedance spectroscopy as a function of water vapor pressure, pH_2O, and demonstrated improved performance with increased pH_2O which was attributed to the insertion of protonic defects ($OH_o^\bullet$) into the structure.[13] Although such behaviour may indicate protonic conductivity in the $LnBaCo_2O_{5+\delta}$ materials, this needs to be established unambiguously, since there is no direct evidence of the presence of structural protons in this family of materials. Due to the sensitivity of neutron diffraction to both light atom positions and site occupancies, we undertook an *in situ* high temperature study in dry and wet (D_2O) argon and wet (D_2O) air on two double perovskite compounds, $NdBaCo_{2-x}Mn_xO_{5-\delta}$ ($x = 0$ and 0.5), using time-of-flight (TOF) neutron powder diffraction (NPD). The aim was to verify their stability and monitor their structural behaviour under operating conditions relevant to H^+-SOFC cathodes. Since the insertion of proton defects into typical proton conducting electrolytes occurs between 300 and 600 °C and dehydration/deprotonation prevails at higher temperatures,[7] isothermal neutron diffraction data were collected in the temperature range of 260–800 °C. The $x = 0.5$ composition has been investigated in order to shed light on the impact of the electronegativity of the *B* cation as well as that of crystal symmetry and oxygen content on the hydration capacity and stability under wet conditions. It is well known that in perovskite type proton conducting electrolytes, the electronegativity of the *B* cation impacts the stabilization of proton defects and any symmetry reduction reduces water solubility.[7] Whereas the symmetry of the $x = 0$ material changes between orthorhombic and tetragonal as a function of temperature and gas atmosphere, the symmetry of the $x = 0.5$ material is tetragonal and remains unchanged on heating/cooling in air or in an inert atmosphere.[17]

2. Experimental

The preparation of the polycrystalline samples ($x = 0$, 0.5) has been described elsewhere.[18] Phase purity was assessed by powder X-ray diffraction (XRD) collected at room temperature over the range $10 \leq 2\theta \leq 120°$, $\Delta 2\theta = 0.02°$ using a Bruker AXS D8 Advance diffractometer in Bragg–Brentano geometry equipped with a Ge primary monochromator (Cu-Kα_1 radiation) and a Lynxeye detector. The initial oxygen content was determined *via* iodometric titration against a standardized sodium thiosulfate solution (~0.05 M). A powder sample (~300 mg) was introduced into a closed argon-flushed glass container and covered by a large excess of KI (~2 g). Approximately 20 mL of hydrochloric acid twice diluted was added to the warm mixture (~40 °C) that was stirred under an argon flow. When dissolution was complete, the iodine formed was titrated under an argon flow with $Na_2S_2O_3$ solution and the calculated oxygen stoichiometry was based on the amount of I_2 formed. Thermogravimetric analysis (TGA) was carried out using a Netzsch STA 449 F3 instrument. Samples weighing ~100 mg, loaded in platinum crucibles, were heated to 800 °C at a rate of 10 °C min^{-1} in 1 atm of dry air (40 mL min^{-1}) before cooling in air at 10 °C min^{-1}. This cycle was performed to clean the sample and remove absorbed free water, hydrates, hydroxides and carbonates. Subsequent cycles were carried out in dry or wet gas, as detailed in Results and discussion.

In situ neutron diffraction data were collected on the high-flux medium resolution POLARIS diffractometer at ISIS, the UK spallation source at the Rutherford Appleton Laboratory. The powder samples were loaded to a height of 4 cm in a double-walled quartz cell which enabled gas to flow through the powder in the neutron beam, and was connected to a panel allowing the switching of gas streams (*e.g.* dry and wet). Two thermocouples were attached on opposite sides of the inner quartz cell wall just above the sample to control and monitor the furnace temperature. The temperature ramp was always 10 °C min^{-1}. The samples were first heated from 20 to 800 °C in dry argon to clean the surface and remove protonic species ($Ba(OH)_2$, $Ba(OH)_2 \cdot nH_2O$, and $Ba(OH)_x(CO_3)_y \cdot nH_2O$) and to increase the amount of oxygen vacancies which may favour the insertion of proton defects. Subsequently, the atmosphere was changed to wet argon then to wet air. A humid atmosphere was generated with D_2O in preference to H_2O (the coherent scattering lengths of H and D are −3.7406 and 6.671 fm, respectively). In addition, the incoherent scattering cross section of D (2.05 barn) is much lower than that of H (80.27 barn).[19] The D_2O injector was connected to the cell and the humidifier was set at 60 °C to provide a saturated vapor pressure, roughly 0.2 bar at atmospheric pressure. Neutron diffraction data were collected on the $x = 0$ and 0.5 samples according to the profiles illustrated in Fig. 1, which were chosen to complement the TGA data.

The main difference in the temperature profiles used for the two compositions lies in more numerous data collected in wet air on $x = 0$ than on $x = 0.5$. Since the former exhibits various phase transitions, we investigated any changes in symmetry/crystal structure, oxygen content or hydroxyl intercalation/

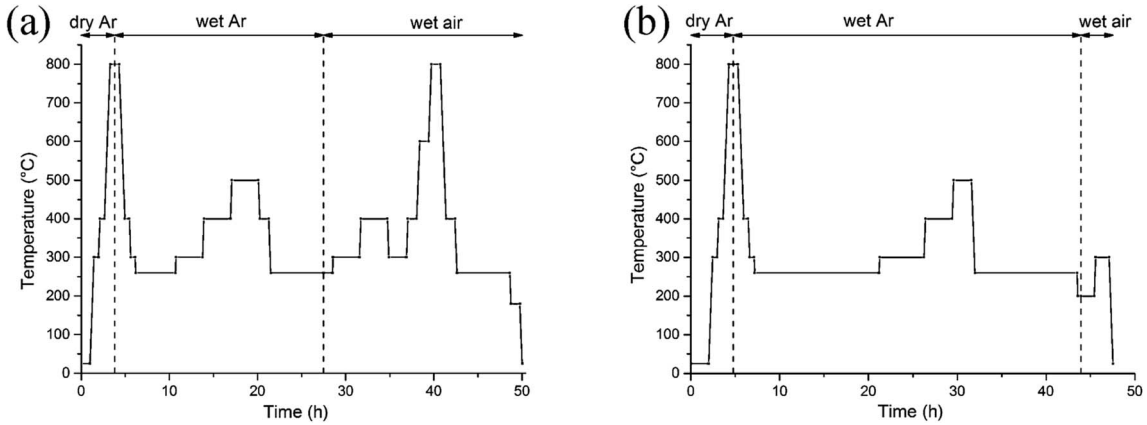

Fig. 1 Temperature profiles for (a) $NdBaCo_2O_{5+\delta}$ and (b) $NdBaCo_{1.5}Mn_{0.5}O_{5+\delta}$.

deintercalation, stability in wet air, kinetics of oxygen exchange and thermodynamic equilibrium as a function of temperature. Data normalisation and file output was performed using the Mantid software package.[20] The patterns from two banks of detectors, the backscattering bank (average $2\theta = 146.7°$, d-spacing range 0.2–2.65 Å) and the 90° bank (average $2\theta = 92.6°$, maximum d-spacing 4.1 Å) were simultaneously fitted by the Rietveld method using the FullProf refinement program.[21] Peak shapes were modeled using the convolution of two back-to-back exponentials with a pseudo-Voigt function. The background due to the amorphous quartz cell was estimated from linear interpolation between manually selected N points ($40 \leq N \leq 70$) chosen to ensure they did not interact with the Bragg reflections of the phase of interest. In addition to the profile parameter (σ_1) describing the Gaussian contribution to the Bragg peak profiles, anisotropic strain broadening parameters (*i.e. hkl* dependent) have been refined through the S_{hkl} microstrain parameters in Stephens' model.[22] The lattice parameters, fractional occupancy of all oxygen sites, atomic positions and atomic displacement parameters (either isotropic or anisotropic) were refined for each pattern. Any additional constraints are noted when describing specific models. Electron diffraction (ED) experiments at room temperature were performed using a Transmission Electron Microscope (TEM) JEOL2100 LaB_6 operating at 200 kV. Powders of $x = 0$ and 0.5 were crushed in dry ethanol and a drop of the suspension was deposited on a copper grid covered by a carbon film. Diffraction patterns were collected with a GATAN Orius 200D Charge Coupled Device (CCD) camera.

3. Results and discussion

3.1. Thermogravimetric analysis

The behaviour of the $x = 0$ and 0.5 compositions was studied by thermogravimetric analysis in wet air ($pH_2O = 0.18$–0.60 atm) to check the influence of the presence of oxygen vacancies on water uptake in these electron conducting phases. Two series of measurements were performed according to the following procedure: the powders were heated in dry N_2 from RT up to 800 °C at a rate of 10 °C min^{-1} followed by isothermal heating at 800 °C for 1 h, in order to achieve thermodynamic equilibrium and maximize the oxygen vacancy content. The sample was then cooled to 260 °C at a rate of 10 °C min^{-1} in dry N_2 and maintained at 260 °C for 1 h. Afterwards, the gas was changed to dry air and after equilibration the sample was stepwise heated to 800 °C before cooling. To check for possible water insertion, a second treatment that consisted of heating/cooling in wet air was performed after the cycle in dry N_2. Thermogravimetric data measured for the $x = 0$ sample are displayed in Fig. 2.

The large mass decrease subsequent to the heating/cooling cycle in dry nitrogen ($\Delta m/m \sim 1.75\%$) corresponding to a loss of ~0.5 oxygen/f.u. suggests the formation of a large number of oxygen vacancies. As soon as the gas was changed to dry air at 260 °C, a sharp mass increase immediately occurred reflecting rapid oxygen exchange, suggesting that the sample recovered its initial oxygen composition ($NdBaCo_2O_{5.5}$). On heating at $T >$ 260 °C, the mass decreased, reflecting rapid reversible oxygen exchange with the atmosphere.

Switching to wet air after the heating/cooling cycle performed in dry N_2 induces an instantaneous mass increase similar to that observed in dry air. After the stepwise heating to 800 °C and subsequent cooling, a small difference in weight with respect to cycling in dry air was observed. The mass of the x

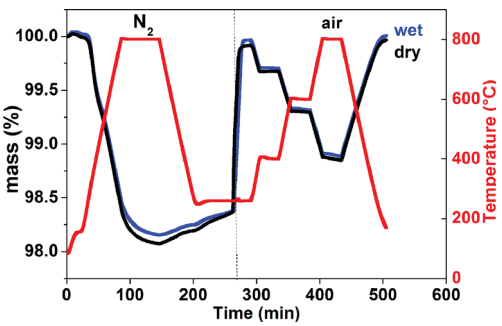

Fig. 2 Thermogravimetric analysis (TGA) of $NdBaCo_2O_{5+\delta}$ in dry N_2 and subsequent heating/cooling cycles in dry (black) or wet (blue) air; the heating/cooling rate is 10 °C min^{-1} and the flow rate is 50 mL min^{-1}. Gas change from N_2 to air at 260 °C is indicated by a vertical dotted line.

= 0.5 sample exhibits little change in dry N_2 reflecting the stability of this composition towards oxygen and humidity when stored under ambient conditions. When heated in air at 260 °C, the behaviour is similar to that of the $x = 0$ sample reflecting immediate chemical oxidation and possible reversible insertion of proton defects (Fig. S.I. 1†).

It is important to stress that the difference in mass between the 'wet' and 'dry' treatments observed for the $x = 0$ and 0.5 samples may indicate the intercalation of proton defects and also reveal the adsorption of free molecules of water and protonic entities such as hydroxide or carbonate. For example, in the XRD pattern of the $PrBaCo_2O_{5+\delta}$ sample hydrated at 500 °C for 12 h in wet air ($pH_2O \sim 0.1$ bar), Grimaud *et al.* showed evidence of the formation of barium carbonate.[13] Since oxidation is the main process that fills the oxygen vacancies of highly deficient double perovskites in wet and dry air, a large oxygen deficiency seems to be not the only requirement for effective proton incorporation in the $LnBaCo_2O_{5+\delta}$ family of materials, likely due to a limited number of lowest energy sites for the protons in this A-site ordered double perovskite layered structure. Indeed, water solubility approaches the saturation limit in cubic perovskite-type proton conducting electrolytes such as $SrTi_{0.95}Sc_{0.05}O_{3-\delta}$,[23] whereas water solubility is reduced in distorted perovskite-type electrolytes and complex perovskites which may exhibit B-site ordering.[23,24] To check the stability of the layered perovskites, $NdBaCo_{2-x}Mn_xO_{5+\delta}$, x = 0 and 0.5 under humid conditions, diffraction experiments have been conducted.

3.2. Structural analysis at room temperature

3.2.1. X-ray diffraction of dry and hydrated $x = 0$ and $x = 0.5$ samples. The powders of the $x = 0$ and $x = 0.5$ samples were heated under dry air from 20 °C to 800 °C at 1 °C min^{-1} and maintained at 800 °C for 1 h before cooling (1 °C min^{-1}) to 20 °C to obtain 'dry' samples. The same thermal profile was carried out in wet air ($pH_2O \sim 0.6$ bar) to obtain 'wet' samples. Both dry and wet samples were confirmed to be single phase by X-ray powder diffraction. The structure of the 'wet' $x = 0$ sample was found to be orthorhombic with the space group *Pmmm* with unit cell data, $a = 3.89048(1)$, $b = 3.90430(1)$, $c = 7.61791(2)$ Å and $V = 115.720(1)$ $Å^3$. The quality of the refinement for the "dry" and "wet" samples was similar, $\chi^2 \sim 1.8$ and ~1.6, respectively. The symmetry of the 'wet' and 'dry' $x = 0.5$ samples was found to be tetragonal with the space group *P4/mmm*; the unit cell data for the wet sample are $a = 3.89691(2)$, $c = 7.65564(4)$ Å and $V = 116.258(2)$ $Å^3$. No major modification appears after heating in wet air in comparison to dry air except a slight increase and decrease in the a and c lattice parameters, respectively. After heating in wet air, the unit cell volumes of the $x = 0$ and 0.5 samples exhibit a small expansion ($\Delta V/V \sim 0.1\%$) with respect to the volume obtained after heating in dry air. The XRD patterns recorded at RT for the $x = 0$ and 0.5 'wet' samples are displayed in Fig. S.I. 2, in the ESI.†

3.2.2. Electron diffraction. Selected Area Electron Diffraction (SAED) patterns of dry $x = 0$ and $x = 0.5$ samples are presented in Fig. 3 for the [100] zone axis. The patterns were indexed according to the pseudocubic unit cell of the perovskite structure.

SAED revealed the existence of two main structural features for the $x = 0$ composition: doubling of two lattice parameters corresponding to an $a_p \times 2a_p \times 2a_p$ supercell, where a_p is the lattice parameter for the cubic perovskite, was observed. The superstructure reflections along c^* have stronger intensities than those along b^*, in agreement with the ordering of the Nd and Ba cations in alternate layers along the c-axis and ordering between oxygen and vacancies along the b-axis in the lanthanide layer, as reported in the literature.[14] For the $x = 0.5$ composition (Fig. 3b), the cation ordering between Nd and Ba cations is retained, whereas oxygen and vacancy ordering along b^* has disappeared likely due to the lower oxygen content due to synthesis under reduced oxygen pressure (*i.e.* argon atmosphere).[18]

3.2.3. Neutron diffraction. The room temperature (RT) Rietveld fit of the neutron powder diffraction (NPD) data for the as-prepared $NdBaCo_2O_{5+\delta}$ ($x = 0$) is displayed in Fig. 4. The pattern can be indexed using the $a_p \times 2a_p \times 2a_p$ unit cell (space group *Pmmm*) as determined by SAED. The doublet at $d \sim 1.95$ Å indexed to 200/040 is consistent with the orthorhombic symmetry and the superstructure low intensity peaks (*e.g.* 014 at $d \sim 1.84$ Å) are associated with the ordering of the oxygen vacancies which occurs when the δ value is close to 0.5.

The orthorhombic crystal structure $a_p \times 2a_p \times 2a_p$ comprises two crystallographically distinct cobalt sites Co1 and Co2 in octahedral and pyramidal coordination, respectively, and seven crystallographically independent oxygen atoms: O1 and O2 in the Ba layer, O3, O4 and O5 at the equatorial positions of the Co polyhedra, and O6 and O7 in the Nd layer (Fig. 5).

The atomic displacement parameters (ADPs) of all the atoms were refined isotropically. Due to high correlations with site occupancy, the ADPs of the oxygen atoms in the same layer were initially constrained to be equal. However, this gave very small values for B_{iso} of the oxygen atoms in the Nd layer (O6 and O7) in comparison to the B_{iso} of the other oxygen atoms.

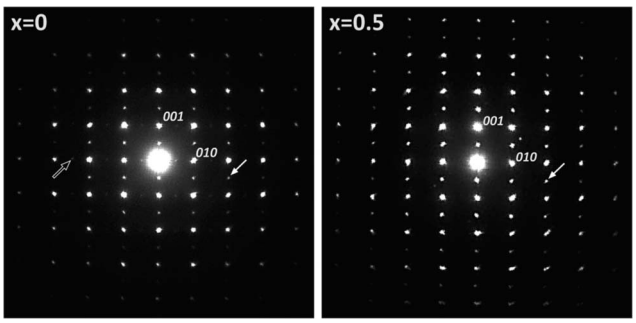

Fig. 3 [100] zone axis electron diffraction patterns of (a) $NdBaCo_2O_{5+\delta}$ ($x = 0$) and (b) $NdBaCo_{1.5}Mn_{0.5}O_{5+\delta}$ ($x = 1.5$). The patterns are indexed considering the cubic parent perovskite unit cell. The white arrows in $x = 0$ and $x = 0.5$ indicate superstructure reflections related to A-site cation ordering along the c-axis, whereas the black arrow in $x = 0$ indicates a superstructure reflection resulting in cell doubling in b due to oxygen vacancy ordering.

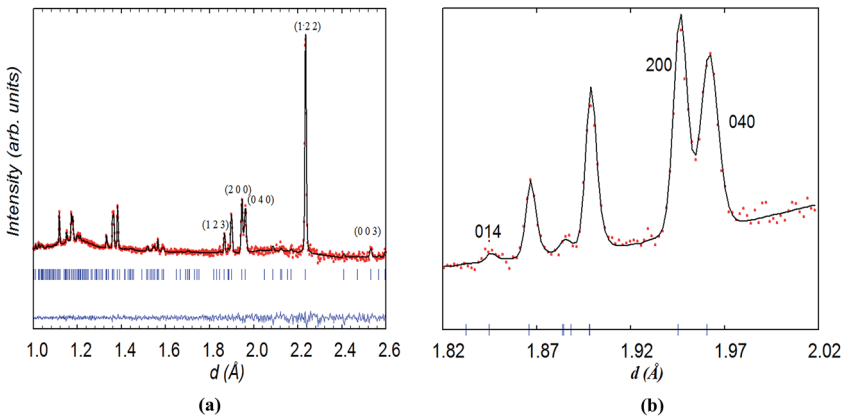

Fig. 4 (a) Rietveld refinement at room temperature from the backscattering bank of $NdBaCo_2O_{5+\delta}$ with (b) an emphasis on 1.82 < d < 2.02 Å showing the superstructure peak of 014 associated with the ordering of the oxygen vacancies. Indexing refers to the ($a_p \times 2a_p \times 2a_p$) cell.

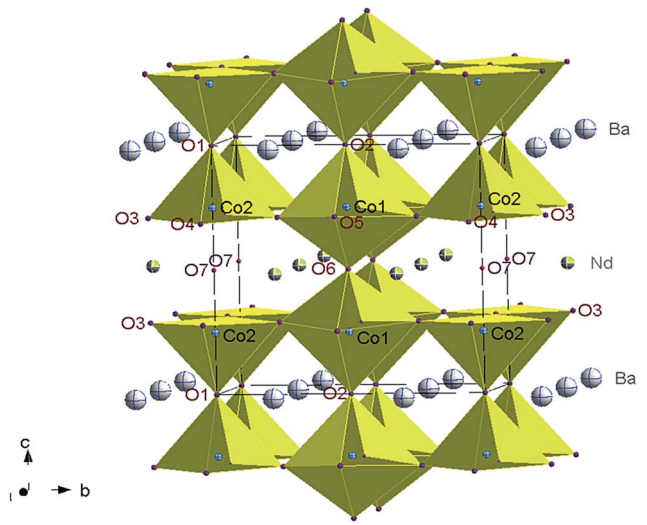

Fig. 5 Crystal structure of $NdBaCo_2O_{5.5}$ highlighting the seven crystallographically distinct oxygen positions. Ordering of oxygen vacancies was observed in the Nd layer, with O6 preferentially occupied and O7 partially occupied.

Consequently, the B_{iso} of all the oxygen atoms were constrained to be equal. The refinement of site occupancies showed that the oxygen vacancies were primarily on one of the two crystallographically independent oxygen sites located in the Nd layers and may exist at the nearest-neighboring O3, O4 and O5 sites in the Co-layer. The difference in site occupancy between O6 [1.00(5)] and O7 [0.20(4)] is consistent with vacancy ordering.[25,26] The occupancy factors of the oxygen sites in the Ba layer (O1 and O2) are within a standard deviation of 1.0 and were therefore fixed to 1.0. Moreover, this value did not vary when the sample was heated/cooled in Ar or air and was therefore maintained fixed in all of the refinements. The total oxygen content corresponded to 5.5(2) atoms/formula unit (f.u.) and agreed with iodometric titration results.[18] Therefore, mainly Co^{3+} ions are present in octahedral CoO_6 and pyramidal CoO_5 environments. The structural parameters of $NdBaCo_2O_{5+\delta}$ at RT are listed in Table 1.

In contrast to $NdBaCo_2O_{5+\delta}$, the symmetry of $NdBaCo_{1.5}Mn_{0.5}O_{5+\delta}$ ($x = 0.5$) at room temperature was found to be tetragonal $P4/mmm$ with the unit cell $a_p \times a_p \times 2a_p$. This model has a single transition metal site for the (Co/Mn) ions and three O sites (O1, O2 and O3). The crystal structure and the Rietveld plot at room temperature are shown in Fig. 6. The excluded region at 1.49 < d < 1.51 Å was introduced for a small bump likely due to an experimental artifact. The mixed B-site possesses weak overall scattering due to the competing Mn and Co scattering lengths, −3.73 and 2.49 fm, respectively. When the ADPs of the mixed site were refined anisotropically, this appeared to cause slightly negative β_{33} for (Co,Mn) and large standard deviations for O1 whose occupancy was very low. Therefore the ADP of (Co/Mn) was refined isotropically and the B_{iso} of O1 was fixed at 0. Refinement results indicated that the majority of vacancies were contained in the Nd layer at the O1 site whose occupancy refined to ~0.088(8), none at the O2 site whose occupancy factor was therefore fixed at 1.0 and very

Table 1 Structural results of $NdBaCo_2O_{5+\delta}$ from neutron powder diffraction data at room temperature

Atom	Position (z), occupation factor (Occ.)	B_{iso} (Å^2)
Nd	y: 0.271(1)	0.74(8)
Ba	y: 0.250(1)	0.7(1)
Co1	z: 0.247(2)	0.7(2)
Co2	z: 0.255(2)	0.3(2)
O1, O2	Occ: *1.00	#1.14(5)
O3	y: 0.2393(1), z: 0.2868(1), Occ: 0.98(2)	#1.14(5)
O4	z: 0.306(2), Occ: 0.94(4)	#1.14(5)
O5	z: 0.268(2), Occ: 0.98(4)	#1.14(5)
O6	Occ: 1.00(5)	#1.14(5)
O7	Occ: 0.20(4)	#1.14(5)
O-content	5.5(2)	

Space group $Pmmm$, a = 3.8914(2) Å, b = 7.84422(44) Å, c = 7.59312(42) Å with sites Nd 2p (0.5 y 0.5), Ba 2o (0.5 y 0), Co1 2r (0 0.5 z), Co2 2q (0 0 z), O1 1a (0 0 0), O2 1e (0 0.5 0), O3 4u (0 y z), O4 2s (0.5 0 z), O5 2t (0.5 0.5 z), O6 1g (0 0.5 0.5), O7 1c (0 0 0.5); # constrained, * fixed, $\chi^2 \sim 0.9$, $R_B \sim 2.8\%$, $R_F \sim 2.8\%$.

little at the O3 site. The overall oxygen content of ~5.00(8)/f.u. corresponds to an equal amount of $(Co,Mn)^{3+}$ and $(Co,Mn)^{2+}$ cations in a square pyramidal coordination. The change from orthorhombic to tetragonal symmetry between the $x = 0$ and $x = 0.5$ compositions and the absence of the superstructure reflections related to vacancy ordering in the latter are consistent with the SAED pattern. The higher symmetry of the $x = 0.5$ compound is due to the presence of a very small amount of oxygen atoms in the Nd-layer due to the annealing conditions in the inert atmosphere required to prevent the stabilization of the hexagonal perovskite $BaMnO_{3-\delta}$ impurity.[18] The R factors and refined structural parameters for $x = 0.5$ at RT are given in Table 2.

Table 2 Structural results obtained from Rietveld fit of neutron powder diffraction data of $NdBaCo_{1.5}Mn_{0.5}O_{5+\delta}$ at room temperature[a]

Atom	Position (z), occupation factor (Occ.)	β_{11}, β_{22}, β_{33} ($\times$ 100)
Nd		1.4(1), 1.4(1), 0.20(6)
Ba		1.3(2), 1.3(2), 0.6(1)
Co,Mn	z: 0.251(2)	*0.7(2)
O1	Occ: 0.088(8)	#0.0 (isotropic)
O2	#Occ: 1.0	1.5(2), 1.5(2), 0.25(8)
O3	z: 0.1981(2), Occ: 0.98(2)	1.6(2), 2.4(2), 0.44(5)
O content	5.00(8)	

[a] Space group $P4/mmm$, $a = 3.9334(1)$ Å, $c = 7.6197(4)$ Å with sites Nd 1a (0 0 0), Ba 1b (0 0 0.5), Co 2h (0.5 0.5 z), O1 1c (0.5 0.5 0), O2 1d (0.5 0.5 0.5), and O3 4i (0.5 0 z), # fixed, * refined isotropically, $\chi^2 \sim 2.1$, R_B ~2.2%, $R_F \sim 3.0\%$.

3.3. Structural analysis as a function of temperature in an argon atmosphere

3.3.1. $NdBaCo_2O_{5+\delta}$. The $NdBaCo_2O_{5+\delta}$ sample was stepwise heated in dry Ar up to 800 °C before switching to wet gas. This heating was performed to dry the sample and maximize the oxygen-ion vacancy content in the lattice as it may favor the incorporation of proton defects. Indeed, for some Ruddlesden–Popper (RP) phases such as $Sr_3FeMnO_{7-\delta}$, increasing the amount of oxygen vacancies by annealing in a N_2 atmosphere at 500 °C was shown to have a positive impact on the hydration reaction, possibly due to kinetics.[27] In the analysis of the data collected above room temperature in an argon atmosphere, isotropic ADPs were refined for all the atoms and for all the oxygen atoms they were constrained to be the same. Isothermal datasets collected for 30 minutes at 300 and 400 °C show insignificant variations in the oxygen content along with the retention of the orthorhombic space group. This agrees with the TGA carried out in a N_2 atmosphere, which indicates mass loss above $T \sim 400$ °C (Fig. 2). At 800 °C, the structure has transformed to tetragonal (S.G. $P4/mmm$); the doublet (040, 200) merged into a single peak and the small peaks associated with oxygen-vacancy ordering have disappeared. The tetragonal structural model used in the refinements of the data collected at 800 °C and on subsequent cooling in wet argon is the same as that used for the $x = 0.5$ composition, illustrated in Fig. 6a. Note that for all the rare-earth double perovskite cobaltites, heating accompanied by decreasing of the oxygen content from 6 to 5 causes a series of structural transformations in the sequence "tetragonal–orthorhombic–tetragonal". For $NdBaCo_2O_{5+\delta}$, the orthorhombic to tetragonal transition was reported to occur at $T \sim 500$ °C according to *in situ* X-ray diffraction in air.[28] The oxygen occupancy remained unchanged in the Ba layer at temperatures of up to 800 °C, whereas it decreased in the Nd layers and at the equatorial positions of the Co polyhedra; at 800 °C, the occupancy of O1 and O3 sites refined to 0.42(5) and 0.88(3), respectively, and the overall oxygen content of ~4.9(2) atoms/f.u. is in good agreement with the value of 5.14(2) measured by Cox-Galhotra *et al.* under similar conditions ($T = 777$ °C, $pO_2 = 10^{-4}$ atm)[29] and with the value reached after the TGA cycle performed in a N_2 atmosphere (Fig. 2). At 800 °C, the gas was switched to wet (40% D_2O/Ar) and the same structural model was used for the dry and hydrated samples. Rietveld analysis of the dataset collected at 800 °C for 30 minutes in wet argon indicated a possible slight decrease in the occupancy of O1 to ~0.32(2) due to incomplete equilibration on holding the sample for 30

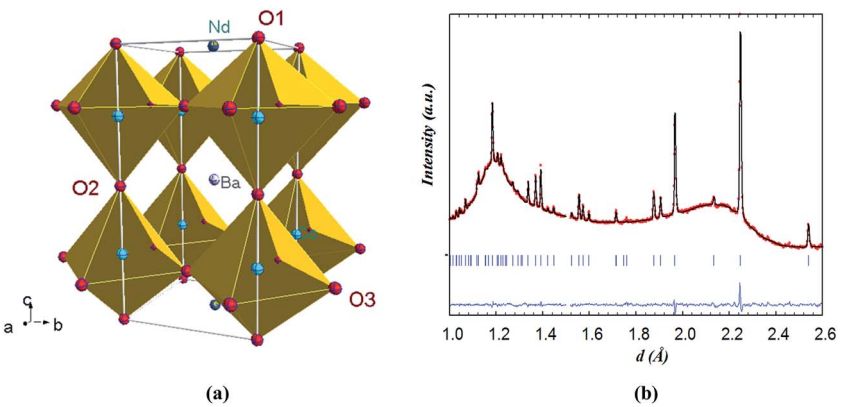

Fig. 6 (a) Crystal structure of $NdBaCo_{1.5}Mn_{0.5}O_{5+\delta}$ ($P4/mmm$) with the transition metals highlighted in blue (b) Rietveld refinement at room temperature from the backscattering data bank. The undulating background is due to the quartz sample environment. The excluded region at $1.49 < d < 1.51$ Å was introduced for a small bump likely due to an experimental artifact.

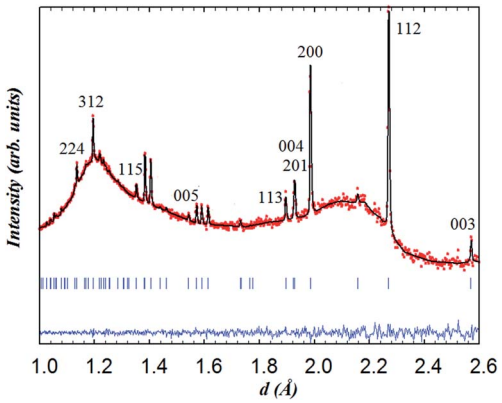

Fig. 7 Rietveld refinement for $NdBaCo_2O_{5+\delta}$ from the data collected from the backscattering bank at 800 °C for 30 min under wet argon. The indexing refers to the ($a_p \times a_p \times 2a_p$) cell. The undulating background is due to the quartz sample environment.

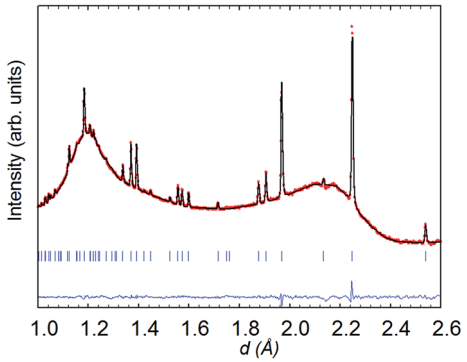

Fig. 8 Rietveld refinement (space group *P4/mmm*) from the backscattering detector bank for $NdBaCo_2O_{5+\delta}$ at 260 °C in wet (40% D_2O) argon; data collected for 6 h.

minutes at 800 °C in dry Ar. Conversely, the occupancy of O3 ~ 0.90(3) remains unchanged within the estimated standard deviations; the overall oxygen content corresponds to 4.9(1) atoms/f.u. Neither structure distortion nor a significant change in the cell parameters between data collected in both dry and wet argon at 800 °C was observed; the same thermodynamic equilibrium appears to be reached on heating in each atmosphere within 30 minutes. Moreover, no additional peaks related to sample decomposition were observed, highlighting the excellent stability of $NdBaCo_2O_{5+\delta}$ under humid conditions in contrast to the double perovskite $Ba_3Ca_{1.18}Nb_{1.82}O_{9-\delta}$ (BCN18) where the presence of secondary phases, mostly hydroxides, was evidenced.[30,31] However, it should be mentioned that if impurities are limited to trace levels, their detection is difficult in diffraction experiments. A Rietveld profile from data recorded at 800 °C in wet argon is shown in Fig. 7 and the relevant structural parameters derived for both dry and wet atmospheres are displayed in Table 3.

The sample was therefore stepwise cooled in wet argon, meanwhile, datasets were collected at different temperatures to allow possible hydration/dehydration to be monitored through the variation of the oxygen content. Rietveld analysis of the datasets collected at relevant temperatures and performed using anisotropic ADPs for the metal positions and isotropic ADPs for the oxygen sites (since anisotropic ADPs gave a negative value of β_{33} for (O1)) did not show significant variation in the oxygen occupancy. Fig. 8 shows the Rietveld fit of the pattern collected at 260 °C, the lowest temperature reached on cooling in wet argon. Relevant structural parameters are given in Table 4.

3.3.2. $NdBaCo_{1.5}Mn_{0.5}O_{5+\delta}$. The thermal evolution of the Mn-substituted composition ($x = 0.5$) in dry argon is very similar to that of the pure cobalt material ($x = 0$), except that there is no orthorhombic → tetragonal phase transition as the Mn-compound is already tetragonal. The temperature dependence of the oxygen stoichiometry, determined from the Rietveld analysis of the data listed in Table 5, indicates that the oxygen content remains close to 5.0/f.u. These results show that there is no influence of the oxygen content, particularly a large oxygen deficiency, on the reactivity of the $NdBaCo_{2-x}Mn_xO_{5+\delta}$ ($x = 0, 0.5$) compounds with water (*i.e.* water dissociation) in wet argon. Conversely, in Ruddlesden–Popper compounds such as

Table 3 Rietveld parameters in dry and wet argon at 800 °C for $NdBaCo_2O_{5+\delta}$ (S.G. *P4/mmm*) with sites Nd 1*a* (0 0 0), Ba 1*b* (0 0 0.5), Co 2*h* (0.5 0.5 *z*), O1 1*c* (0.5 0.5 0), O2 1*d* (0.5 0.5 0.5), and O3 4*i* (0.5 0 *z*). The ADPs of the metals were refined anisotropically and B_{iso} for the oxygen atoms was constrained to be the same

$NdBaCo_2O_{5+\delta}$	Dry Ar, 800 °C	Wet Ar, 800 °C
a (Å)	3.9657(3)	3.9712(4)
c (Å)	7.7179(8)	7.7117(9)
Co (*z*)	0.246(3)	0.249(2)
O3 (*z*)	0.2091(7)	0.2063(6)
Occ. O1	0.42(5)	0.32(2)
Occ. O3	0.88(3)	0.90(3)
O-content	4.9(2)	4.9(1)
χ^2	0.65	0.7
R_B%	4.2	3.7
R_F%	10.8	11.3

Table 4 Structural parameters of $NdBaCo_2O_{5+\delta}$ (S.G. *P4/mmm*) at 260 °C in 40% D_2O/Ar[a]

Atom	Position (*z*), occupation (Occ.)	β_{11}, β_{22}, β_{33} (× 100)
Nd		2.3(1), 2.3(1), 0.54(5)
Ba		2.0(2), 2.0(2), 0.45(7)
Co	*z*: 0.2468(7)	1.9(2), 1.9(2), 0.51(7)
O1	Occ: 0.264(8)	#1.72(4)
O2		#1.72(4)
O3	*z*: 0.2035(2), Occ: 0.944(8)	#1.72(4)
O-content	5.04(4)	

[a] Space group *P4/mmm*, $a = 3.9349(1)$ Å, $c = 7.6197(3)$ Å with sites Nd 1*a* (0 0 0), Ba 1*b* (0 0 0.5), Co 2*h* (0.5 0.5 *z*), O1 1*c* (0.5 0.5 0), O2 1*d* (0.5 0.5 0.5), O3 4*i* (0.5 0 *z*), # B_{iso} constrained to be equal, $\chi^2 \sim 2.2$, $R_B \sim 3\%$, $R_F \sim 3.7\%$.

Table 5 Oxygen occupancy of $NdBaCo_{1.5}Mn_{0.5}O_{5+\delta}$ determined from neutron diffraction data in wet argon. The occupancy factor for O2 was fixed at 1.0. Collection time is indicated in parenthesis[a]

T (°C) atom	800 (30 min)	260 (14 h)	300 (5 h)	400 (3 h)	500 (2 h)	260 (11 h)	200 (20 min)
O1	0.072(8)	0.072(0)	0.080(8)	0.072(8)	0.064(8)	0.080(8)	0.064(8)
O3	0.95(4)	0.98(1)	0.99(2)	0.97(2)	0.96(2)	0.99(2)	0.97(3)
O-content/f.u.	4.9(2)	4.98(5)	5.03(7)	4.94(7)	4.90(8)	5.03(7)	5.0(1)

[a] Refinement with anisotropic ADPs for all the atoms except B_{iso} for (Co,Mn) and $B_{iso} = 0$ for O1.

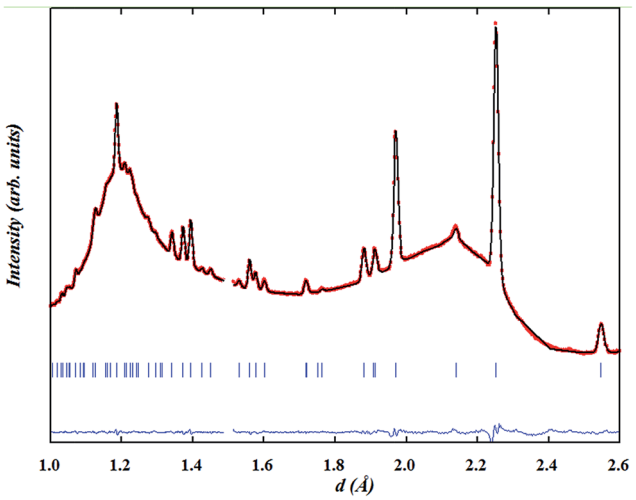

Fig. 9 Rietveld profile (backscattering detector bank) for $NdBaCo_{1.5}Mn_{0.5}O_{5+\delta}$ in wet argon at 260 °C; data collected for 11 h; refinement with anisotropic ADPs for all the atoms except for (Co,Mn) for which B_{iso} was refined and B_{iso} for O1 fixed at 0.

$Sr_3Fe_2O_{7-\delta}$ and $PrSr_3Co_{1.5}Fe_{1.5}O_{10-\delta}$, the oxygen stoichiometry (δ) considerably influences the hydration properties.[27,32,33]

Fig. 9 displays the Rietveld refinement of the data collected for 11 h at 260 °C in wet argon with Table 6 listing the corresponding structural parameters.

The behaviour of the $x = 0.5$ sample in dry and wet argon is governed by thermal expansion and exhibits some hysteresis at low temperature (*e.g.* at 260 °C) likely due to low equilibration. The evolution of the structural parameters is displayed in Fig. S.I. 3.†

Table 6 Structural parameters of $NdBaCo_{1.5}Mn_{0.5}O_{5+\delta}$ (S.G. *P4/mmm*) at 260 °C in 40% D_2O/Ar

Atom	Position (z), occupancy (Occ.)	β_{11}, β_{22}, β_{33} ($\times$ 100)
Nd		1.9(1), 1.9(2), 0.28(5)
Ba		1.7(2), 1.7(2), 0.7(1)
Co,Mn	z: 0.252(2)	#0.7(2)
O1	Occ: 0.080(8)	*$B_{iso} = 0$
O2		2.3(2), 2.3(2), 0.32(7)
O3	z: 0.1986(2), Occ: 0.99(2)	2.0(2), 2.6(2), 0.81(5)
O-content	5.03(7)	

Refined isotropically. * Fixed.

3.4. Structural evolution in wet air

3.4.1. $NdBaCo_2O_{5+\delta}$. As soon as the gas was changed from wet argon to wet air at 260 °C, the single-phase model no longer gave a satisfactory fit to the data collected on the $x = 0$ sample. The presence of extra peaks clearly evidenced the growth of a second phase. Fig. 10 shows the datasets collected in the temperature range of 260–800 °C. The changes were mainly observed in the (200) Bragg peak (index corresponding to the *P4/mmm* symmetry), which is almost the only reflection available to monitor the evolution of the initial phase and the new one. The other peaks overlap due to the similarity in the structures and compositions of the two phases.

The data collected at 260 °C for 1 h were initially fitted with two tetragonal phases with different lattice parameters and oxygen contents; however, the model did not resemble the observed pattern well with the reliability factors: global $\chi^2 \sim 1.45$, $R_B \sim 8.0\%$, $R_F \sim 5.6\%$ for phase 1 and $R_B \sim 3.0\%$, $R_F \sim 4.6\%$ for phase 2. The use of two orthorhombic phases yielded lower reliability factors: global $\chi^2 \sim 1.0$, $R_B \sim 5.7\%$, $R_F \sim 4.8\%$ for phase 1 and $R_B \sim 3.0\%$, $R_F \sim 4.4\%$ for phase 2. It is interesting to mention that using a single orthorhombic phase resulted in a higher reliability factor, $\chi^2 = 1.8$.

In contrast to the *Pmmm* structural model ($a_p \times 2a_p \times 2a_p$) which fits the data of the as-prepared material at RT and on heating in dry Ar up to 400 °C, the *Pmmm* model ($a_p \times a_p \times 2a_p$)

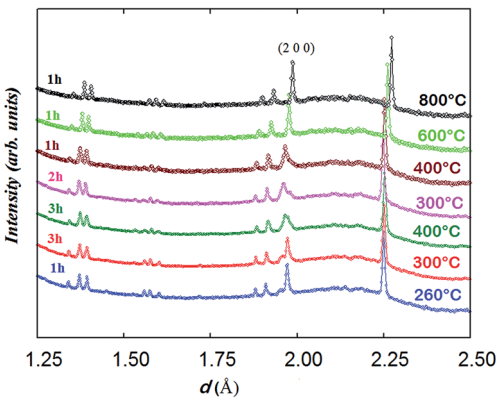

Fig. 10 Evolution of the NPD patterns (backscattering detector bank) of $NdBaCo_2O_{5+\delta}$ obtained in wet air from 260 to 800 °C, index corresponds to the *P4/mmm* symmetry. The two orthorhombic phases co-exist in the temperature range of 260–400 °C; the collection duration of each dataset is indicated; time increases upwards.

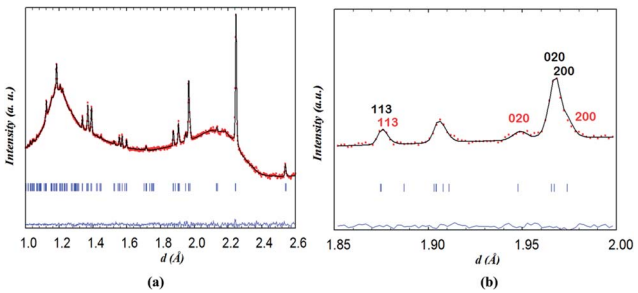

Fig. 11 (a) Two-phase fit of neutron diffraction data collected on $NdBaCo_2O_{5+\delta}$ for 1 h at 260 °C in wet air and (b) emphasis on the contributions of (black) phase 1 and (red) phase 2.

that assumes disordered vacancies and consists of a single Co site and four different oxygen sites O1, O2, O3 and O4 was used in the two-phase refinements due to the large number of parameters and similarity of the two phases. All the sites were refined with isotropic ADPs. Due to the low occupancy at the O1 site in the Nd layer and similar symmetry to the O2 site in the Ba layer, B_{iso} for O1 and O2 was constrained to be identical. Due to strong correlations between B_{iso} and site occupancy for O3 and O4 (which are localized at the equatorial positions of the Co polyhedra and accommodate very little oxygen vacancies), B_{iso}, occupancy and z positions of O3 and O4 were constrained to be the same in each phase. Relaxing these constraints did not change the quality of the refinement. The refinement of two strain broadening parameters, S_{400} and S_{040}, was needed to fit accurately the data collected during the intercalation process and must be constrained to be equal for the two banks and the two phases to allow sensible evolution of the weight ratios as a function of time. The O3/O4 sites in phase 2 (oxidised phase) were found to be fully occupied and their occupancy was fixed at 1.0 in all of the two-phase refinements. Oxygen vacancies were mainly localised at the O1 site in the two phases although less in phase 2 than in phase 1. The distortion of the basal plane of the intercalated phase (phase 2) at 260 °C (a = 3.94483(7), b = 3.8960(8) Å) whose oxygen content refined to 5.5(2) atoms/f.u. is more pronounced than in the initial phase 1 (a = 3.9345(8), b = 3.9315(9) Å) whose oxygen-content refined to 4.9(1) atoms/f.u. In addition, the c parameter of phase 2 is larger than that in phase 1, 7.633(2) *vs.* 7.6181(6) Å, in agreement with the larger oxygen content (or proton defects) in the former. The fit of the pattern collected for 1 h at 260 °C in wet air is displayed in Fig. 11.

Heating above 260 °C enhances the nucleation and growth of the phase 2 whose δ value remains almost constant, at ~0.5(2) in the temperature range of 260–400 °C. The oxygen content of phase 1 increases with time although it remains lower than that of phase 2 as illustrated in Fig. 12c. After 7 hours of heating in wet air, the two phases have a similar weight ratio and an "inversion" of the orthorhombicity is produced; the a and b lattice parameters of phase 2 which were significantly different at 260 °C become similar at 400 °C (a =

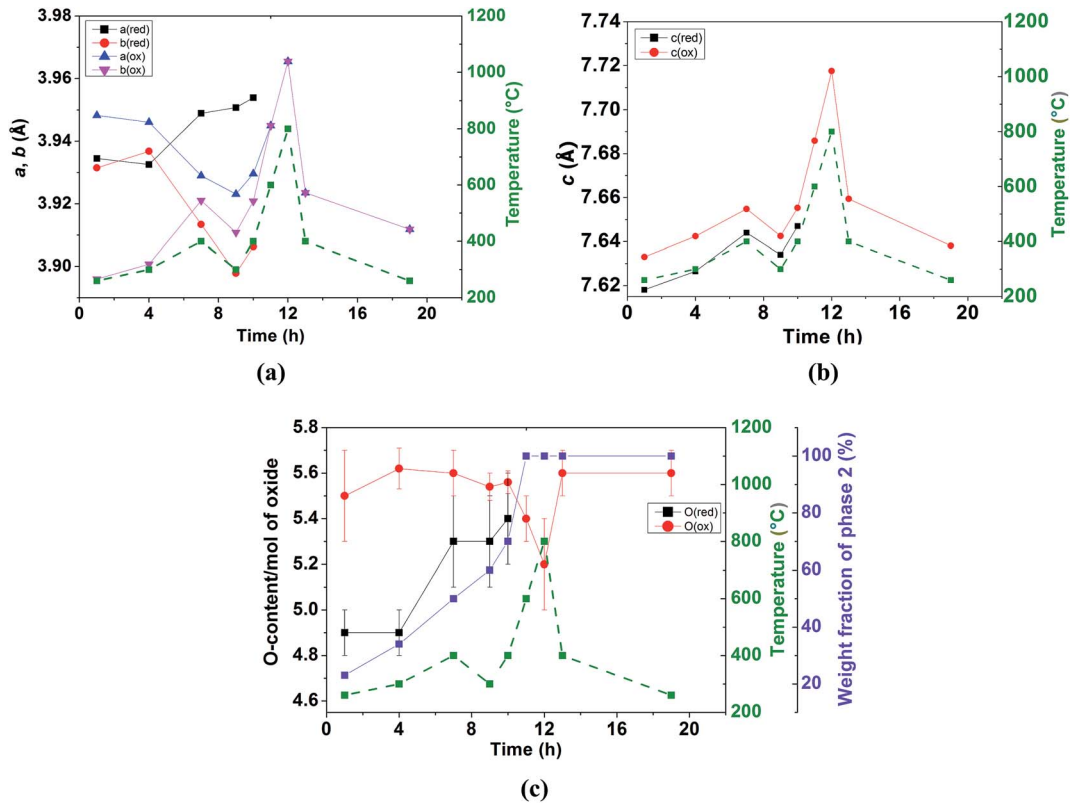

Fig. 12 Structural variation of $NdBaCo_2O_{5+\delta}$ (x = 0) in wet air; (a) a and b lattice parameters, (b) c lattice parameter (c) oxygen content and weight fraction of phase 2; (red) and (ox) relate to phases 1 and 2, respectively.

Table 7 Main results of the Rietveld refinements in *P4/mmm* for $NdBaCo_{1.5}Mn_{0.5}O_{5+\delta}$ in wet air[a]; collection time is indicated in parenthesis

	Phase 1	Phase 2
200 °C (1 h 30 min)		
a (Å)	3.9380(2)	3.9179(4)
c (Å)	7.6421(5)	7.6685(2)
Occ. O1	0.056(8)	0.40(6)
Oxygen content	5.12(2)	5.8(1)
Weight fraction (%)	80(5)	20(5)
300 °C (1 h 30 min)		
a (Å)	3.9405(5)	3.9090(2)
c (Å)	7.653(2)	7.6809(5)
Occ. O1	0.17(4)	0.42(2)
Oxygen content	5.33(8)	5.82(3)
Weight fraction (%)	20(5)	80(5)

[a] The occupation of O3 and O4 have been fixed at 1.0.

3.929(4) and b = 3.921(4) Å), whereas phase 1 which was pseudo tetragonal at 260 °C (a = 3.9345(8) and b = 3.9315(9) Å) becomes significantly orthorhombic at 400 °C (a = 3.949(1) and b = 3.9134(9) Å) as shown in Fig. 12a. This behavior may be due to the increased oxygen content in both phases (Fig. 12c) and possible ordering of the oxygen vacancies in phase 1 whose δ value approaches 0.5. The evolution of the c lattice parameters is mainly governed by thermal expansion (Fig. 12b) rather than chemical expansion consecutive to variations in the oxygen content and shows the presence of some hysteresis (*e.g.* at 400 °C). The c lattice parameter of phase 2 remains larger than that of phase 1, in agreement with the larger oxygen content in the former. Heating at 600 °C promotes the intercalation reaction kinetically and the two phases merge into a single tetragonal phase with $\delta \sim 0.4(2)$, suggesting that the oxygen transport at 600 °C is sufficiently rapid to overcome the kinetic limitations experienced at lower temperatures. The sample remains in a single tetragonal phase at 800 °C and on subsequent cooling. No secondary phases were detected at any temperature. In the temperature range of the coexistence of the two phases, the sample undergoes a fast intercalation reaction between an oxygen deficient ($\delta \sim 0$) and an oxygen rich phase ($\delta \sim 0.5(2)$). Variation of the cell parameters, oxygen content and weight fractions is displayed in Fig. 12.

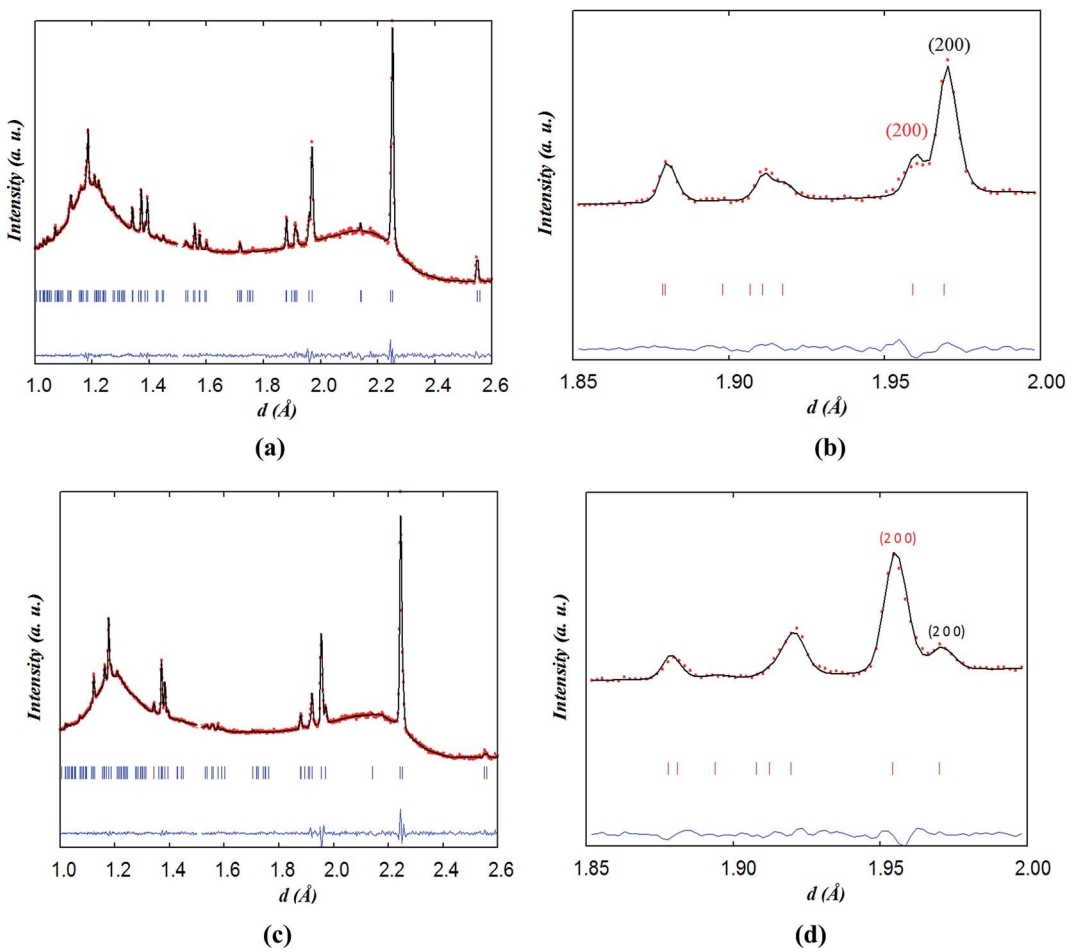

Fig. 13 Two-phase fits for neutron data collected on $NdBaCo_{1.5}Mn_{0.5}O_{5+\delta}$ in wet air for 90 minutes at (a and b) 200 °C and (c and d) 300 °C using a tetragonal model; (red) intercalated and (black) reduced phases.

3.4.2. $NdBaCo_{1.5}Mn_{0.5}O_{5+\delta}$. The behavior of the $x = 0.5$ composition in wet air is similar to that of the $x = 0$ phase and indicates the growth of an intercalated oxidised phase. Only two datasets were collected in wet air at this composition, at 200 and 300 °C. In contrast to the two-phase orthorhombic model used to fit the data collected on the $x = 0$ composition, a two-phase tetragonal model was used to fit these data. The reliability factors χ^2 for the two-phase model are 2.6 and 2.1 at 200 and 300 °C, respectively, in comparison to $\chi^2 = 4.9$ and 3.9 when a single tetragonal phase is used.

The two-phase tetragonal model consistent with the diffraction pattern recorded at 200 and 300 °C for 90 minutes is shown in Fig. 13. The main results of the Rietveld refinements are displayed in Table 7. At 200 °C, the smaller *a*- and larger *c*-lattice parameters of phase 2 (oxidised phase) with respect to phase 1 (reduced phase) are consistent with the larger oxygen content in the former. This behaviour is exhausted at 300 °C where the proportion of phase 2 has reached ~80%.

The reason for the existence of the two phases during the exposure of the $x = 0$ and 0.5 samples to wet air may stem from the two accessible values of δ for the $NdBaCo_2O_{5+\delta}$ and $NdBaCo_{1.5}Mn_{0.5}O_{5+\delta}$ compositions, close to 0.0 and 0.5 with a portion of the sample oxidizing preferentially. The need for two phases to fit the data collected in wet air for 10 h up to 400 °C on the $x = 0$ sample may indicate that the kinetics of oxidation are relatively slow and that the oxidation process is limited for the time that the samples were held at each temperature between 260 and 400 °C (1–3 hours) because of the low flow rate of the gas (20 mL min^{-1}) and the large quantity of the powder sample used in the neutron experiment (~4 g). Conversely, the TGA experiment, using a smaller quantity of sample (100 mg) and higher flow rate (50 mL min^{-1}), would suggest that the surface exchange and diffusion of oxygen are fast in the reduced phase under these conditions.

Although our diffraction experiment highlighted the stability of the layered phases of $x = 0$ and 0.5 under humid conditions, it was difficult to establish the incorporation of proton defects into this oxide family. Water dissociation strongly depends on the basicity of the ceramics and the presence of the Ba cation at the A site. This basicity is however lowered by the substitutions with less basic elements such as Nd which prevent the reaction with acidic gases such as H_2O and therefore hydrolysis. It is worthwhile stressing that despite intensive studies on systems that insert a large amount of proton defects, such as the brownmillerite $Ba_2In_2O_5$ and derived compositions[34,35] and orthorhombic perovskite $BaCe_{0.9}Y_{0.1}O_{2.95}$ [36] or cubic $La_{0.73}Ba_{0.27}ScO_{2.865}$ [37] or $SrZr_{0.95}Sc_{0.05}O_{3-\delta}$[38] perovskites, the determination of the proton site is only suggested at very low temperatures, far from the conducting conditions. It should be mentioned that the improvement of the electrochemical properties of the layered cobaltite $PrBaCo_2O_{5+\delta}$ with increased pH_2O reported by Grimaud *et al.*[13] can be related to the formation of secondary phases such as hydroxides which are very good proton conductors and consequently did not reflect the properties of their bulk materials. Indeed, Jalarvo *et al.*[39] showed by *in situ* synchrotron X-ray diffraction that in the case of the proton conducting perovskites, $Sr_4(Sr_2Nb_2)O_{11}\cdot nH_2O$ and $Sr_4(Sr_2Ta_2)O_{11}\cdot nH_2O$, secondary phases such as $Sr(OH)_2$ can dominate proton conduction.

4. Conclusion

The vacancy ordered $NdBaCo_{2-x}Mn_xO_{5+\delta}$ ($x = 0$, 0.5) layered perovskites have been investigated in dry and wet argon and wet air by *in situ* high temperature neutron powder diffraction. The materials were found to be stable under strongly humid conditions up to 800 °C. However, the incorporation of proton defects could not be clearly established from our *in situ* data collected under wet conditions as a function of temperature. This suggests that the basic characteristics of the $NdBaCo_{2-x}Mn_xO_{5+\delta}$ phases owing to the Ba cation along with the presence of large amount of oxygen deficiencies and high oxygen mobility which are the key factors involved in the mechanism of water dissociation/insertion in cubic perovskite proton conducting electrolytes (*e.g.* acceptor-doped barium zirconates and cerates) appear not to be the most relevant factors for water dissociation/incorporation in the ordered Co-based double perovskites studied.

Acknowledgements

One of the authors (M. B.) thanks P. D. Battle (Oxford University) and T. Roisnel (University of Rennes) for much helpful advice during the course of the refinements as well as G. Gauthier (Industrial University of Santander) and F. Tonus (Imperial College London) who provided with very valuable comments. The authors also thank R. Haynes and the rest of the sample environment team at ISIS for their assistance. This research was partially supported by the ANR IDEA-MAT grant (ANR-A2-BS08-0012-01) which provided a Post-doctoral Fellowship for J. Hanlon.

References

1 D. J. L. Brett, A. Atkinson, N. P. Brandon and S. J. Skinner, *Chem. Soc. Rev.*, 2008, **37**, 1568–1578.
2 S. C. Singhal and K. Kendall, *High Temperature Solid Oxide Fuel Cells: Fundamentals, Design and Applications*, Oxford, 2003.
3 B. C. H. Steele and A. Heinzel, *Nature*, 2001, **414**, 345–352.
4 C. Zuo, S. Zha, M. Liu, M. Hatano and M. Uchiyama, *Adv. Mater.*, 2006, **18**, 3318–3320.
5 H. Iwahara, *Solid State Ionics*, 1996, vol. 86–88, Part 1, pp. 9–15.
6 H. Iwahara, T. Yajima, T. Hibino and H. Ushida, *J. Electrochem. Soc.*, 1993, **140**, 1687–1691.
7 K. D. Kreuer, *Annu. Rev. Mater. Res.*, 2003, **33**, 333–359.
8 K. D. Kreuer, *Solid State Ionics*, 1997, **97**, 1–15.
9 T. Norby, *Solid State Ionics*, 1999, **125**, 1–11.
10 B. Lin, S. Zhang, L. Zhang, L. Bi, H. Ding, X. Liu, J. Gao and G. Meng, *J. Power Sources*, 2008, **177**, 330–333.
11 H. Uchida, S. Tanaka and H. Iwahara, *J. Appl. Electrochem.*, 1985, **15**, 93–97.

12 G. Goupil, T. Delahaye, B. Sala, F. Lefebvre Joud and G. Gauthier, *Solid State Ionics*, 2014, **263**, 15–22.
13 A. Grimaud, F. Mauvy, J. M. Bassat, S. Fourcade, L. Rocheron, M. Marrony and J. C. Grenier, *J. Electrochem. Soc.*, 2012, **159**, B683–B694.
14 A. Maignan, C. Martin, D. Pelloquin, N. Nguyen and B. Raveau, *J. Solid State Chem.*, 1999, **142**, 247–260.
15 A. Tarancon, S. J. Skinner, R. J. Chater, F. Hernandez-Ramirez and J. A. Kilner, *J. Mater. Chem.*, 2007, **17**, 3175–3181.
16 A. Tarancón, A. Morata, G. Dezanneau, S. J. Skinner, J. A. Kilner, S. Estradé, F. Hernández-Ramírez, F. Peiró and J. R. Morante, *J. Power Sources*, 2007, **174**, 255–263.
17 K. V. Kordesch and G. R. Simader, *Chem. Rev.*, 1995, **95**, 191–207.
18 T. Broux, M. Bahout, J. M. Hanlon, O. Hernandez, S. Paofai, A. Berenov and S. J. Skinner, *J. Mater. Chem. A*, 2014, **2**, 17015–17023.
19 V. F. Sears, *Neutron News*, 1992, **3**, 26–37.
20 Mantid, *Manipulation and Analysis Toolkit for Instrument Data. Mantid Project*, 2013.
21 J. Rodríguez-Carvajal, *Phys. B*, 1993, **192**, 55–69.
22 P. W. Stephens, *J. Appl. Crystallogr.*, 1999, **32**, 281–289.
23 K. D. Kreuer, *Solid State Ionics*, 1999, **125**, 285–302.
24 A. S. Nowick and Y. Du, *Solid State Ionics*, 1995, **77**, 137–146.
25 S. Streule, A. Podlesnyak, E. Pomjakushina, K. Conder, D. Sheptyakov, M. Medarde and J. Mesot, *Phys. B*, 2006, **378–380**, 539–540.
26 J. C. Burley, J. F. Mitchell, S. Short, D. Miller and Y. Tang, *J. Solid State Chem.*, 2003, **170**, 339–350.
27 M. Lehtimaki, H. Yamauchi and M. Karppinen, *J. Solid State Chem.*, 2013, **204**, 95–101.
28 J. H. Kim, L. Mogni, F. Prado, A. Caneiro, J. A. Alonso and A. Manthiram, *J. Electrochem. Soc.*, 2009, **156**, B1376–B1382.
29 R. A. Cox-Galhotra, A. Huq, J. P. Hodges, J.-H. Kim, C. Yu, X. Wang, A. J. Jacobson and S. McIntosh, *J. Mater. Chem. A*, 2013, **1**, 3091–3100.
30 I. Sosnowska, R. Przeniosło, W. Schäfer, W. Kockelmann, R. Hempelmann and K. Wysocki, *J. Alloys Compd.*, 2001, **328**, 226–230.
31 T. Shimoyama, T. Tojo, H. Kawaji, T. Atake, N. Igawa and Y. Ishii, *Solid State Ionics*, 2008, **179**, 231–235.
32 L. Jantsky, H. Okamoto, A. Demont and H. Fjellvåg, *Inorg. Chem.*, 2012, **51**, 9181–9191.
33 M. Matvejeff, M. Lehtimäki, A. Hirasa, Y. H. Huang, H. Yamauchi and M. Karppinen, *Chem. Mater.*, 2005, **17**, 2775–2779.
34 V. Jayaraman, A. Magrez, M. Caldes, O. Joubert, F. Taulelle, J. Rodriguez-Carvajal, Y. Piffard and L. Brohan, *Solid State Ionics*, 2004, **170**, 25–32.
35 I. Ahmed, C. S. Knee, M. Karlsson, S. G. Eriksson, P. F. Henry, A. Matic, D. Engberg and L. Börjesson, *J. Alloys Compd.*, 2008, **450**, 103–110.
36 K. S. Knight, *Solid State Ionics*, 2001, **145**, 275–294.
37 E. Kendrick, K. S. Knight, M. S. Islam and P. R. Slater, *Solid State Ionics*, 2007, **178**, 943–949.
38 T. Ito, T. Nagasaki, K. Iwasaki, M. Yoshino, T. Matsui, N. Igawa and Y. Ishii, *Solid State Ionics*, 2006, **177**, 2353–2356.
39 N. Jalarvo, C. Haavik, C. Kongshaug, P. Norby and T. Norby, *Solid State Ionics*, 2009, **180**, 1151–1156.